THE JOURNAL OF PHYSICAL CHEMISTRY B

ARTICLE

pubs.acs.org/JPCB

Molecular Simulation of Aqueous Electrolyte Solubility. 2. Osmotic Ensemble Monte Carlo Methodology for Free Energy and Solubility Calculations and Application to NaCl

Filip Moučka,[†,‡] Martin Lísal,[‡,⊥] Jiří Škvor,[†,∥] Jan Jirsák,[†,§,⊥] Ivo Nezbeda,[§,⊥] and William R. Smith[*,†]

[†]Faculty of Science, University of Ontario Institute of Technology, Oshawa, ON L1H7K4, Canada

[‡]Department of Physics, [§]Department of Chemistry, and [∥]Department of Informatics, Faculty of Science, J. E. Purkinje University, 400 96 Ústín. Lab., Czech Republic

[⊥]E. Hála Laboratory of Thermodynamics, Institute of Chemical Process Fundamentals of the ASCR, v. v. i., 165 02 Prague 6, Czech Republic

ABSTRACT: We present a new and computationally efficient methodology using osmotic ensemble Monte Carlo (OEMC) simulation to calculate chemical potential−concentration curves and the solubility of aqueous electrolytes. The method avoids calculations for the solid phase, incorporating readily available data from thermochemical tables that are based on well-defined reference states. It performs simulations of the aqueous solution at a fixed number of water molecules, pressure, temperature, and specified overall electrolyte chemical potential. Insertion/deletion of ions to/from the system is implemented using fractional ions, which are coupled to the system via a coupling parameter λ that varies between 0 (no interaction between the fractional ions and the other particles in the system) and 1 (full interaction between the fractional ions and the other particles of the system). Transitions between λ-states are accepted with a probability following from the osmotic ensemble partition function. Biasing weights associated with the λ-states are used in order to efficiently realize transitions between them; these are determined by means of the Wang−Landau method. We also propose a novel scaling procedure for λ, which can be used for both nonpolarizable and polarizable models of aqueous electrolyte systems. The approach is readily extended to involve other solvents, multiple electrolytes, and species complexation reactions. The method is illustrated for NaCl, using SPC/E water and several force field models for NaCl from the literature, and the results are compared with experiment at ambient conditions. Good agreement is obtained for the chemical potential−concentration curve and the solubility prediction is reasonable. Future improvements to the predictions will require improved force field models.

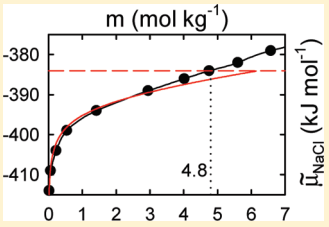

1. INTRODUCTION

The development of computationally efficient algorithms for the molecular level simulation of aqueous electrolyte solutions is an important problem, both because of its fundamental interest and because of the important role of these systems in industrial, geochemical, and biological applications.[1] Such simulations not only complement experimental observations, but also provide molecular level insight that can contribute to the development of thermodynamic models for their correlation and prediction.[2] Among the most important properties are electrolyte chemical potentials and solubility; these quantities are the focus of this series of papers.

Most previous simulation studies of aqueous electrolyte solutions have been performed using closed system ensembles, in which the number of particles of each species (N_i) is fixed; these have been particulary the constant-volume, constant-temperature (NVT) ensemble or the constant-pressure, constant-temperature (NPT) ensemble, using both Monte Carlo (MC) and molecular dynamics (MD) methods (V is the system volume, T is the temperature, P is the pressure, and $N = \Sigma_i N_i$ is the total number of particles). Typical goals of these studies have been to calculate structural, dynamical, and volumetric properties at ambient conditions,[3,4] in addition to conditions of high pressure and temperature.[5] Applications have typically been made to alkali halides, with emphasis on simpler electrolytes such as NaCl.

When entropic or free-energy properties such as chemical potential or Gibbs free energy of solvation are of interest, they have typically been determined in simulations by thermodynamic integration,[6] expanded ensemble methods (e.g., refs 7, 8), or free energy perturbation and other methods (e.g., ref 9). Knowledge of the electrolyte chemical potential, μ, as a function of concentration (typically molality, m) is important (herein referred to as a $\mu-m$ curve), both in its own right and as an indirect means of determining electrolyte solubility, as the concentration at which the total electrolyte chemical potential is equal to that of the corresponding crystalline solid.[10] This approach for determining aqueous electrolyte solubility using NPT MD simulations has been used by Cui and Harris,[11] who studied the solubility of NaCl in steam and in supercritical water; by Ferrario et al.,[12] who determined the solubility of KF; and by Sanz and Vega,[13] who

Received: March 3, 2011
Revised: April 21, 2011
Published: May 31, 2011

dx.doi.org/10.1021/jp202054d | J. Phys. Chem. B 2011, 115, 7849–7861

determined the solubility of KF and NaCl (the latter two studies were at near-ambient conditions.) For the crystalline solid, Cui and Harris separately evaluated its chemical potential by means of a quasiharmonic approximation,[14] while Ferrario et al. and Sanz and Vega evaluated it in their simulations using the Frenkel−Ladd thermodynamic integration technique.[15] Recently, Paluch et al.[16] presented an adaptable method to simulate the solubility limit of solids. The method uses a MC expanded isothermal−isobaric ensemble for the solution phase to compute chemical potentials and an MD approach using the pseudosupercritical path integration method to calculate the free energy of the solid. They calculated the solubility of NaCl in water and in alcohols at ambient conditions.

In a recent study, Joung and Cheatham[17] directly computed the solubilities of alkali−halide electrolytes in water in closed ensemble *NPT* MD simulations, using a periodic orthorhombic box with coexisting crystal and ions in solution. The solubility was measured as the concentration of ions in the solution phase remote from the solid−liquid interface. This method is computationally very demanding, since it requires the use of a large system to suppress finite-size effects and long simulation runs to reach a true solid−liquid equilibrium. In addition, the method relies on using the same intermolecular potential model for both solid and solution phases. They also calculated activity coefficients using thermodynamic integration.

In contrast to closed ensembles, simulations of aqueous electrolyte solutions in open ensembles,[18] such as the osmotic ensemble MC (OEMC) approach, where the species concentrations are determined as averages over a simulation run performed at chemical potentials specified in some way (see details in the Methodology section of this work), can in principle greatly facilitate simulations of the solubility and $\mu-m$ curves. For the former, the ion solute concentration in equilibrium with the solid can be determined directly as that resulting from the imposition of the specified overall external solid chemical potential; for the latter, since the imposed chemical potential can be continuously varied, the $\mu-m$ curve can be readily calculated over a continuous range by essentially calculating its inverse function. Another advantage of the OEMC approach over the use of a closed ensemble simulation is its superior accessibility of the low concentration range. Whereas the computational demands of OEMC simulations are relatively independent of concentration, in a closed ensemble the lowest concentration that can be simulated is a mole fraction of $1/(N_s + 1)$, where N_s is the number of solvent molecules. Since computationally feasible N_s values are currently only the order of several hundred, the simulation of systems with lower concentrations imposes significant computational requirements.

The determination of the value of the chemical potential of the solid is a problem that can be separated from that of determining the chemical potentials of its ions in solution. Our approach assumes the former to be known; this is the case for many solids, whose values are given in thermochemical tables. Our approach hence avoids any errors introduced in this aspect of a solubility calculation. When the solid chemical potential is unknown, it must be evaluated separately. Either empirical methods of estimation (e.g., ref 19) must be used or it must also be determined by separate computer simulation techniques. We remark that such simulations may require different force field models than those used for the ions in aqueous solution.

Notwithstanding the suggested advantages of the OEMC approach, its implementation entails significant technical challenges. The primary problem is that simulations in open ensembles rely on insertion/deletion of particles to/from the system (free energy calculations in closed ensembles also share this challenge.) In the case of aqueous electrolyte solutions, such insertion/deletion of ions has proven to be an extremely challenging computational problem. Direct (Widom-like) insertion/deletion of several ions at once (e.g., a cation and an anion for an aqueous 1:1 electrolyte solution, as required by electroneutrality) has virtually zero probability at ambient conditions. For example, simultaneous insertion of Na^+ and Cl^- ions into pure water at ambient conditions is accompanied by a typical free-energy change of about 300 k_BT, where k_B is Boltzmann's constant; such a direct insertion corresponds to a probability of about 5×10^{-131}. The deletion of a pair of ions is similarly unlikely.

In the first paper of this series,[18] we developed an expanded ensemble osmotic molecular dynamics (EEOMD) approach, which combined MD *NPT* simulation with a MC approach at specified electrolyte chemical potential and applied it to a 1:1 electrolyte. We alleviated the insertion/deletion problem by incrementally coupling/decoupling the ions (hereafter called fractional ions) to/from the system, by means of a coupling parameter λ that varied between 0 (no interaction between the fractional ions and the other particles in the system) and 1 (full interaction between the fractional ions and the other particles in the system). The transition between $\lambda = 0$ and $\lambda = 1$ was effected by means of scaling and biasing procedures. The λ-coupling approach to mimic insertion/deletion of particles or molecules is not new; Escobedo and de Pablo appear to have been the first to use it, in their so-called expanded ensemble grand canonical MC method.[20] The method has been extensively used in grand canonical MD (GCMD) simulations[21] and also more recently by us in mesoscopic simulations.[22] The gradual coupling/decoupling of inserted particles to/from the system is also a key element of the so-called continuous fractional component (CFC) MC method proposed by Shi and Maginn[23] for open system atomistic simulations.

In addition to λ-coupling, for complex systems like the aqueous electrolyte solutions considered in this work, a biasing technique that facilitates transitions between neighboring λ-states is also necessary; without such a strategy, in extreme cases the system may become trapped at intermediate states (see, e.g., ref 20). The biasing technique associates with each λ-value a biasing factor (biasing weight), chosen in such a way that the free-energy differences between neighboring λ-states are reasonably small (and hence neighboring state transition probabilities are reasonable). Unlike previous implementations of the biased λ-coupling approach, such as for the systems considered by the CFC MC method[23] (simple dense fluid, ambient water, and carbon dioxide−ethanol systems), where the use of biasing factors improves the computational efficiency, their use is crucial for more complex systems such as aqueous electrolyte solutions. Inserting/deleting ions to/from water cannot be accomplished without a careful choice of both a λ-coupling procedure and corresponding biasing factors. Furthermore, due to the global electroneutrality of the system, aqueous electrolyte solutions require inserting/deleting several ions to/from water at once.

Biasing factors have been customarily determined to achieve visits of all λ-states with uniform probability (the flat histogram

approach).[20] Recently, Trebst et al.[24] have proposed an alternative strategy, whereby the biasing factors are chosen to maximize the number of round trips between states with $\lambda = 0$ and $\lambda = 1$ (the optimum histogram approach).[25] The latter methodology has been recently refined by Escobedo and Martnez-Veracoechea in their MinTau and Min2Tau methods.[26] In our EEOMD method,[18] we estimated biasing factors by a combination of short thermodynamic integration and optimization steps based upon the Wilding and Müller iterative updating scheme.[27] Determination of the biasing factors must be done prior to a production run, and for our EEOMD method this turned out to be very time-consuming. In addition, the biasing factors were somewhat dependent on concentration, and further readjustment was necessary for different concentration ranges. Although the EEOMD method gave consistent results when compared with closed-ensemble simulations and the method allowed the direct simulation of solubility in principle, the associated computational overhead due to the determination of the biasing factors drastically reduced the overall efficiency of the method. In the CFC MC method,[23] Shi and Maginn proposed using automatic determination and adaptive adjustment of the biasing factors using Wang−Landau sampling.[28] This is a key advance over our previous EEOMD approach.

The purpose of this paper is to present a new OEMC method for the computationally efficient calculation of properties involving free energy for aqueous electrolyte solutions that improves upon previous implementations and is tailored for the systems of interest. This permits the efficient calculation of $\mu-m$ curves and the direct calculation of solubility. It is formulated in a general way that views the calculation as the simulation of an interphase chemical reaction, directly linking our approach to the reaction ensemble Monte Carlo (RxMC) method.[29] It avoids calculations involving the solid phase and issues with respect to the choice of reference states, instead using readily available free energy values in compilations such as the NIST-JANAF[30] or Thermodynamics Research Center tables.[31] We develop our general approach and apply it to an aqueous NaCl solution at ambient conditions, as a prototypical example of an aqueous 1:1 electrolyte solution.

The method simulates the system at a fixed number of water molecules, pressure, temperature, and overall electrolyte chemical potential. The approach draws upon concepts from both the EEOMD and the CFC MC methods, including generalizing the concept of fractional ions from the former. The method uses, similarly as in the CFC MC approach, the concept of automatic determination and adaptive adjustment of the biasing weights based on the Wang−Landau sampling technique, as refined and modified for the systems of interest. We also propose a generalized λ-coupling procedure that can be used for both nonpolarizable and polarizable molecular models and that can be efficiently used with the generalized reaction field (GRF) approach[32] for treating the long-ranged Coulombic interactions.

Use of the GRF approach for treating Coulombic interactions is generally computationally preferable over the standard Ewald summation (ES) technique.[15,33] Also, in contrast to the GRF method, when the ES technique is used, the interactions between the periodic images of the ions might cause spurious artifacts;[32] this is particularly the case for multiple ion insertion/deletion, when these ions can create a large dipole moment in each periodic image. Nevertheless, we also use the ES approach at a few state points to make comparison with our simulations utilizing the GRF approach. We also compare our results with experimental data for NaCl at ambient conditions and with the results of previous authors.

The reminder of the paper is organized as follows. The derivation and computational background considerations of the OEMC methodology are presented in section 2. Section 3 describes the molecular models used, and section 4 summarizes the simulation details. The results are presented and discussed in section 5, and the final section contains our conclusions.

2. METHODOLOGY

In this section, we present the overall details of the OEMC approach (section 2.1), followed by a discussion of technical implementation details (section 2.2).

2.1. Osmotic Ensemble Simulation and Solubility Calculations. We develop a formalism for osmotic ensemble MC simulations of a solution containing t species at specified pressure P and temperature T, where the particle numbers of a subset of species are fixed and the chemical potentials of the s remaining species are specified in some way. A primary goal is to calculate the concentrations of the latter species.

From basic statistical mechanics,[34] the probability of occurrence of a configuration in such a system with $\{N_i, i = 1, 2, ..., t\}$ molecules, in a volume V, with reduced particle positions and molecule rotations, $\xi^N \equiv \xi_j$ and $\omega^N \equiv \omega_j$, respectively, $j = 1, ..., \sum_{k=1}^{t} N_k$, is proportional to

$$\left[\prod_{i=1}^{t}\frac{1}{N_i!}\left(\frac{Vq_i}{\Lambda_i^3}\right)^{N_i}\right]\exp\{-\beta[U(\xi^N,\omega^N)+PV-\sum_{i=1}^{t}\mu_i N_i]\} \quad (1)$$

where $\beta = 1/(k_B T)$, and μ_i, q_i, and Λ_i are the chemical potential per particle, internal partition function, and thermal de Broglie wavelength of species i, respectively.

According to the Metropolis scheme,[33] a Markov chain is constructed in which a sequence of configurations is generated by incrementally changing positions, rotations, system volume, and particle counts, $\{N_i\}$. The positions, rotations, and volume are changed in the standard way as in the case of NPT simulation. The $\{N_i\}$ values for the species with specified chemical potentials are changed according to a transition probability which at steady state yields their average values. The transition probability $\Pi(i \rightarrow j)$ for performing a MC step to change the particle counts by $\{\Delta N_i\}$ (resulting in a change in system configurational energy U by ΔU) is given by the ratio of terms in eq 1:

$$\Pi(i \rightarrow j) = \min\left\{1; \left[\prod_{i=1}^{s}\frac{N_i!}{(N_i+\Delta N_i)!}\left(\frac{Vq_i}{\Lambda_i^3}\right)^{\Delta N_i}\right]\exp[-\beta(\Delta U-\sum_{i=1}^{s}\mu_i\Delta N_i)]\right\} \quad (2)$$

The q_i term is related to the standard molar chemical potential of species i, $\tilde{\mu}_i^0(T,P^0)$,[35] via

$$\frac{q_i}{\Lambda_i^3} = \beta P^0 \exp(-\beta\mu_i^0) = \beta P^0 \exp\left(-\beta\frac{\tilde{\mu}_i^0}{N_A}\right) \quad (3)$$

where μ_i^0 is the standard chemical potential per particle of species i, N_A is Avogadro's number, and P^0 is the standard-state pressure (typically taken to be 1 bar). Accurate and readily available values

for $\tilde{\mu}_i^0$ are available in thermochemical compilations such as the NIST-JANAF[30] or Thermodynamics Research Center tables.[31] By inserting eq 3 into eq 2, the transition probability can be expressed as

$$\Pi(i \rightarrow j) = \min\left\{1; \left[\prod_{i=1}^{s} \frac{N_i!}{(N_i + \Delta N_i)!}(V\beta P^0)^{\Delta N_i}\right] \exp[-\beta(\Delta U + \Delta G^{\mathrm{P}})]\right\} \quad (4)$$

where

$$\Delta G^{\mathrm{P}} = -\sum_{i=1}^{s} (\mu_i - \mu_i^0)\Delta N_i \quad (5)$$

is interpreted as the externally prescribed free energy driving force of the MC step changing $\{N_i\}$ by $\{\Delta N_i\}$. Equations 4 and 5 provide the general transition probabilities for the OEMC method.

In the special case when the $\{\Delta N_i\}$ are governed by a chemical reaction (involving the s species and other thus far unspecified species)

$$\sum \nu_i A_i = 0 \quad (6)$$

where $\{\nu_i\}$ are stoichiometric coefficients and $\{A_i\}$ denotes the species involved, and the $\{\Delta N_i\}$ satisfy

$$\Delta N_i = \nu_i \Delta\xi \qquad i = 1, \ldots, s \quad (7)$$

where $\Delta\xi$ is an extent of reaction parameter for eq 6. Equation 5 then becomes

$$\Delta G^{\mathrm{P}} = -\left(\sum_{i=1}^{s} \nu_i(\mu_i - \mu_i^0)\right)\Delta\xi \quad (8)$$

This allows the OEMC method to be used to determine compositions subject to a specified chemical reaction involving an externally specified $\Sigma\, \nu_i\mu_i$ term (as, for example, across a phase boundary or a semipermeable membrane).

In our case, an aqueous 1:1 electrolyte solution involving ions A^+ and B^- in equilibrium with its solid AB(s) corresponds to equilibrium for the chemical reaction

$$\mathrm{AB(s)} = \mathrm{A^+(aq)} + \mathrm{B^-(aq)} \quad (9)$$

corresponding to eq 6. Equilibrium for reaction 9 is achieved when (henceforth for notational convenience we omit the (aq) description for the ions)

$$\mu_{\mathrm{AB(s)}} = \mu_{\mathrm{A^+}} + \mu_{\mathrm{B^-}} \quad (10)$$

corresponding to $\nu_A = \nu_B = 1$, $s = 2$ for $\Delta\xi = +1$ in eq 7. $\Sigma\, \nu_i\mu_i$ from eq 10 is substituted in eq 8 to yield the final result:

$$\Delta G^{p} = (\mu_{\mathrm{A^+}}^0 + \mu_{\mathrm{B^-}}^0 - \mu_{\mathrm{AB(s)}})\Delta\xi \quad (11)$$

$\Delta\xi = +1$ corresponds to insertion of the ions and $\Delta\xi = -1$ corresponds to deletion. The OEMC method employing the transition probability of eq 4 in conjunction with eq 11 may thus be viewed as an implementation of the RxMC method for the interphase chemical reaction of eq 9.

2.2. λ-Coupling Approach. As previously mentioned, the acceptance ratio for direct insertion/deletion of ions in an aqueous solution is virtually zero, and as a result the simulation becomes trapped at a given concentration, where N_i cannot change. We circumvent this problem by a combination of two strategies. First, we gradually insert/delete the ions via a sequence of values of a coupling parameter λ_j, corresponding to intermediate states (or fractional particles). Second, we ensure that MC transitions between neighboring states are reasonably likely by assigning biasing weights to the states. The first involves the selection of a scaling procedure that defines the λ states and specifies a functional form that implements the overall process of ion pair insertion between the initial and final states corresponding to $\lambda = 0$ and $\lambda = 1$, respectively. The second strategy using biasing weights may be a convenience in other situations, but in the case at hand, it is essential in ensuring that the simulation does not become trapped at an intermediate state.

We define a general equilibrium process P involving an initial and final state and a prescribed free energy driving force ΔG^{P}:

$$\text{initial state} \overset{\Delta G^{\mathrm{P}}}{\rightleftharpoons} \text{final state} \quad (12)$$

The initial and final states can be respectively identified with an ion pair decoupled from the solution and a pair fully immersed in the solution (corresponding to $\Delta\xi = 1$ in eq 11) or with the reverse process ($\Delta\xi = -1$). Our following discussion will assume the case $\Delta\xi = +1$. To make the MC sampling of P more efficient, we break it into subprocesses, which represent transitions between neighboring λ-states corresponding to fractional particles (frac part.), i.e.,

$$\text{initial state}(\lambda_0 = 0) \overset{\Delta G_0^{\mathrm{P}}}{\rightleftharpoons} \text{frac part.}(\lambda_1) \overset{\Delta G_1^{\mathrm{P}}}{\rightleftharpoons} \text{frac part.}(\lambda_2)\ldots \overset{\Delta G_{M+1}^{\mathrm{P}}}{\rightleftharpoons} \text{final state}(\lambda_{M+2} = 1) \quad (13)$$

where

$$\Delta G^{\mathrm{P}} = \sum_{j=0}^{M+1} \Delta G_j^{\mathrm{P}} \quad (14)$$

Selection of the particular values of $\{\lambda_j\}$ and M is referred to as a choice of λ-staging. The individual driving forces, $\{\Delta G_j^{\mathrm{P}}\}$, can be chosen arbitrarily subject to eq 14; a particular choice affects the efficiency of the λ-coupling approach. An optimum choice of these parameters depends on the systems and state conditions studied, and general discussion concerning this issue can be found in refs 25 and 26.

In a MC simulation of the process, each MC step corresponding to a subprocess (λ-change) in eq 13 obeys the transition probability of eq 4. For generating the positions of new particles and for insertion/deletion of particles, several schemes are possible. We use the following approach:

(1) We choose $\Delta\xi = \pm 1$ with equal probability for all subprocesses. If a particle is to be deleted, it is chosen randomly from the set of particles with that λ value.
(2) The first subprocess (corresponding to the transition from λ_0 to λ_1) involves the random insertion of a noninteracting ion pair into the simulation box.
(3) The final subprocess (corresponding to the transformation from λ_{M+1} to λ_{M+2}) involves the conversion of a fractional ion pair with $\lambda = 1$ to full ions at $\lambda = 1$.
(4) For all other subprocesses, the position of the new particle is taken from the position of the deleted particle; the new particle's rotation is generated randomly.

This scheme, applied with eq 4, obeys detailed balance.[33]

2.2.1. Scaling of Fractional Ions. For nonpolarizable models, ion−water interactions are typically modeled as a

sum of Lennard-Jones (LJ) and Coulombic potentials located at given sites

$$u_{ij} = 4\varepsilon_{ij}\left[\left(\frac{\sigma_{ij}}{r_{ij}}\right)^{12} - \left(\frac{\sigma_{ij}}{r_{ij}}\right)^{6}\right] + \frac{q_i q_j}{4\pi\varepsilon_0 r_{ij}} \quad (15)$$

where r_{ij} is the distance between the interaction sites, ε_{ij} and σ_{ij} are the corresponding LJ cross parameters, q_i and q_j are the corresponding charges, and ε_0 is the permittivity of vacuum. Ion−ion interactions are modeled either by eq 15 or by the Born−Mayer−Huggins−Tosi−Fumi (BMHTF) potential:

$$u_{ij} = A_{ij}\exp\left(-\frac{r_{ij}}{\rho_{ij}}\right) - \frac{C_{ij}}{r_{ij}^{6}} - \frac{D_{ij}}{r_{ij}^{8}} + \frac{q_i q_j}{4\pi\varepsilon_0 r_{ij}} \quad (16)$$

where A_{ij}, ρ_{ij}, C_{ij}, and D_{ij} are the BMHTF potential parameters.

In previous applications of λ-coupling,[12,21,23] the LJ and Coulombic interactions were both scaled as

$$u(r,\lambda) = \lambda^k u(r) \quad (17)$$

where k is a positive constant, or by means of the scaling procedure of Beutler et al.,[36] originally devised to avoid singularities and instabilities in free energy calculations. For eq 15, Beutler et al. scaled the LJ part of the potential as

$$u_{LJ}(r_{ij},\lambda) = \lambda^k 4\varepsilon_{ij}\left\{\frac{1}{\left[\alpha_{LJ}(1-\lambda)^2 + \left(\frac{r_{ij}}{\sigma_{ij}}\right)^s\right]^{12/s}} - \frac{1}{\left[\alpha_{LJ}(1-\lambda)^2 + \left(\frac{r_{ij}}{\sigma_{ij}}\right)^s\right]^{6/s}}\right\} \quad (18)$$

and the Coulombic part as

$$u_{Coul}(r_{ij},\lambda) = \lambda^k \frac{q_i q_j}{4\pi\varepsilon_0\left[\alpha_{Coul}(1-\lambda)^2 + r_{ij}^{\,p}\right]^{1/p}} \quad (19)$$

where $s > 1$, $p > 1$, and α_{LJ}, and α_{Coul} are positive constants. We found that the simple scaling approach of eq 17 is unsatisfactory for our systems. On the basis of the approach of Beutler et al., we used a general scaling procedure that can be implemented not only for LJ and Coulombic potentials but also for the BMHTF potential and for polarizable models.

Our scaling procedure employs the choice of λ-staging $\lambda_{j+1} = \lambda_j + \Delta\lambda$, and the two following approaches are applied simultaneously: (i) scale the interaction potential by a coupling parameter λ, which is the product of individual coupling parameters $\lambda^{(i)}$ and $\lambda^{(j)}$ of the interacting molecules i and j, i.e., $\lambda = \lambda^{(i)}\lambda^{(j)}$, and (ii) add a term of the form $[R_s(1-\lambda)]^2$ to the squared distance between the interacting sites, r^2. The scaled site−site interaction potential then becomes

$$u(r,\lambda) = \lambda u(r^*) \quad (20)$$

where

$$r^* = \{r^2 + [R_s(1-\lambda)]^2\}^{1/2} \quad (21)$$

In eq 20, u is a general potential of any form, and the parameter R_s in eq 21 was chosen in such a way as to achieve roughly evenly distributed acceptance ratios for all intermediate λ-states. The proposed scaling procedure is similar to and retains the advantages of that of Beutler et al.[36] Note that eqs 20 and 21 give the scaling of Beutler et al. with $k = 1$, $s = 2$, $p = 2$, $\alpha_{LJ} = (R_s/\sigma_{ij})^2$, and $\alpha_{Coul} = R_s^{\,2}$.

2.2.2. Biasing Technique. Due to the large free-energy change associated with the insertion/deletion of ions to/from aqueous solutions, some λ-states may never occur, and the λ-sampling results in a trapped configuration. To circumvent this problem, a common practice is to set biasing factors η_j associated with each λ_j in such a way as to obtain a uniform occurrence of the λ-states (the flat histogram approach).[20] The biasing factors are closely related to the prescribed driving forces ΔG_j^P. However, instead of η_j, we prefer to use biasing weights w_j, expressed in units of energy that are related to ΔG_j^P by

$$\Delta G_j^P = w_j - w_{j-1} + (\lambda_j - \lambda_{j-1})\Delta G^P \quad (22)$$

with $w_0 = w_{M+2}$, ensuring that eq 14 is satisfied. The last term in eq 22 guarantees that ΔG^P is uniformly distributed between the λ-states when all w_j are identical.

Similarly as for the CFC MC method,[23] we utilize the Wang−Landau (WL) approach[28] to set the values of w_j by means of an iterative process. In the WL method, all values of w_j are initially set to zero, $w_j = 0$. During the equilibration period, when the system visits state λ_j, the corresponding value of w_j is increased according to

$$w_j := w_j + \Delta w \quad (23)$$

The parameter Δw is initially set to a value that provides reasonable convergence of the histograms of the λ-states during the first iteration. The histograms are then collected, and when the relative occurrences of all λ-states become reasonably high, the histograms are zeroed, Δw is divided by two, and the process repeated. The iterations are stopped when Δw meets a specified lower threshold. In addition, after each WL iteration a constant is added to all values of w_j to set their average to zero. This prevents numerical overflow of the w_j-values without affecting the relative occurrence of the λ-states. For other details, see the original paper.[28]

The WL approach results in a relatively flat distribution of the λ-states (ensuring all λ-states are visited with roughly equal probability during the simulation). A general rule of thumb for an efficient MC step is to maintain its acceptance ratio at about 0.5;[33] a useful guide is thus to select a λ-staging strategy for a given scaling procedure that achieves this.

3. MOLECULAR MODELS

We tested the OEMC methodology for aqueous solutions of the ions Na^+ and Cl^-, corresponding to the strong electrolyte NaCl(s). We modeled water by the SPC/E force field[37] and used representative models for the water−ion and ion−ion interactions. The SPC/E force field models interactions between two water molecules as the sum of LJ interactions between oxygen atoms and Coulombic interactions between charges via

$$U_{\alpha\beta}^{w-w} = 4\varepsilon_{OO}\left[\left(\frac{\sigma_{OO}}{r_{ij}}\right)^{12} - \left(\frac{\sigma_{OO}}{r_{ij}}\right)^{6}\right] + \sum_{a=1}^{3}\sum_{b=1}^{3}\frac{q_a q_b}{4\pi\varepsilon_0 r_{ab}} \quad (24)$$

The values of the potential parameters together with the geometry are given in Table 1.

dx.doi.org/10.1021/jp202054d |J. Phys. Chem. B 2011, 115, 7849–7861

Table 1. Lennard-Jones Well-Depth (ε), Size (σ), and Charges (q) for Water Atoms and Sodium and Chloride Ions, Together with the Water Geometry[a]

SPC/E H_2O[37]						
LJ interaction	ε/k_B (K)	σ (Å)		q (e)	geometry	
O − O	78.20	3.166	O	−0.8476	O − H	1.00 Å
			H	+0.4238	H − O − H	109.47 deg

LJ interaction	ε/k_B (K)	σ (Å)	charge	q (e)
		Model 1[17]		
Na^+-Na^+	177.457 4	2.159 538	Na^+	+1.0
Cl^--Cl^-	6.433 703	4.830 453	Cl^-	−1.0
Na^+-Cl^-	33.789 17	3.494 996		
Na^+-O	117.801 4	2.662 769		
Cl^--O	22.430 24	4.799 852		
		Model 2[13]		
Na^+-O	71.525 13	2.758	Na^+	+1.0
Cl^--O	62.729 77	3.783	Cl^-	−1.0
		Model 3[44]		
Na^+-Na^+	65.42	2.350	Na^+	+1.0
Cl^--Cl^-	50.32	4.400	Cl^-	−1.0
Na^+-Cl^-	57.375 38	3.375		
Na^+-O	71.52 513	2.758		
Cl^--O	62.729 77	3.783		

[a] k_B is Boltzmann's constant.

Table 2. Parameters of the Born−Mayer−Huggins−Tosi−Fumi Potential A_{ij}, ρ_{ij}, C_{ij}, and D_{ij} for Ion−Ion Interactions in Model 2[a]

interaction	$A/k_B \times 10^{-6}$ (K)	ρ (Å)	$C/k_B \times 10^{-4}$ (K Å^6)	$D/k_B \times 10^{-4}$ (K Å^8)
Na^+-Na^+	4.9156	0.317	1.2168	0.5794
Na^+-Cl^-	14.5620	0.317	8.1121	10.0677
Cl^--Cl^-	40.4426	0.317	84.0184	168.7610

[a] k_B is Boltzmann's constant.

In the first model (hereafter called model 1), the Na^+ and Cl^- ions are treated as charged LJ particles, and the interactions between the water atoms and the ions and between the ions were modeled by a sum of LJ and Coulombic potentials (eq 15). We used the potential parameters from Joung et al.,[17] which reasonably reproduce various experimental properties such as activity coefficients, diffusion coefficients, residence times of atomic pairs, association constants, and solubility; the model parameters are summarized in Table 1. In the second model (hereafter called model 2), the interactions between the water atoms and the ions are also represented by a sum of LJ and Coulombic potentials, while the ion−ion interactions are treated using the BMHTF potential (eq 16). The potential parameters were those used by Sanz and Vega[13] and by Paluch et al.[16] in their indirect simulations of NaCl solubility in ambient water and are listed in Tables 1 and 2. In our previous work,[18] we used Smith and Dang's model[44] (hereafter called model 3), which employs the same ion−water parameters as for model 2 and the ion−ion interactions modeled by LJ potentials.

In all cases, the cross LJ parameters ε_{ij} and σ_{ij} are expressed using the Lorentz−Berthelot mixing rules[33]

$$\varepsilon_{ij} = \sqrt{\varepsilon_i \varepsilon_j}$$
$$\sigma_{ij} = \frac{\sigma_i + \sigma_j}{2} \tag{25}$$

where ε_k and σ_k are the LJ well-depth and size of a site or an ion.

4. SIMULATION DETAILS

Our simulations were applied to aqueous NaCl solutions at T = 298.15 K and P = 1 bar. We used 270 water molecules in a cubic simulation box with periodic boundary conditions. The number of ion pairs in the box varied between 0 and 29. We used the same value of the cutoff radius for both the LJ and Coulombic interactions, r_c = 9 Å. Initially, the particles were placed on an fcc lattice and rotations of the water molecules were generated randomly. The initial configuration was then equilibrated using a standard *NPT* MC simulation.[33] The probabilities of performing particular MC steps were set at 0.005, 0.1, 0.1, 0.4, and 0.395 for volume changes, λ changes, fractional ion translations, ions/water translations, and water rotations.

For the λ-scaling used in this work (eqs 20 and 21) we found by trial and error that R_s = 2.5 Å gave roughly optimal performance. For the WL method, $\Delta w/k_B$ was initially set to 1.81 K and histograms were zeroed when the relative occurrence of every λ-state exceeded 0.7. Iterations were terminated when $\Delta w/k_B$ became less than 7×10^{-4} K. Values of w_j were adjusted for each OEMC run. We used a λ-staging strategy of 20 equally spaced λ values ($\Delta\lambda$ = 0.05), and the resulting acceptance ratios for λ-changes were around 0.5.

We primarily used the generalized reaction field (GRF) method[32] to treat the Coulombic long-range interactions. In the GRF method, the Coulombic pair interaction, u_{Coul}^{GRF}, is given by

$$u_{Coul}^{GRF}(r_{ij}) = \frac{q_i q_j}{4\pi\varepsilon_0 r_{ij}} p\left(\frac{r_{ij}}{r_c}\right)\Phi(r_c - r_{ij}) + C \tag{26}$$

where r_c is the cutoff radius, Φ is the Heaviside step function, and $p(x)$ is a screening polynomial defined by

$$p(x) = (1-x)^4\left(1 + \frac{8x}{5} + \frac{2x^2}{5}\right) \tag{27}$$

In the case of electrically neutral systems, the total potential energy is independent of the constant C. For molecular models such as the three-site water model used here, interactions between sites within the same molecule must be subtracted from the total Coulombic energy, similarly as for the correction of self-interaction for the Ewald summation.[15] The GRF method was implemented with tinfoil boundary conditions. The λ-scaling procedure (eqs 20 and 21) was applied to eq 26.

At a few state points, we also used the ES technique for treatment of the electrostatic interactions, in order to make comparison with the GRF method. For the ES technique, we used the Ewald convergence parameter α = 0.35 Å^{-1} and maximum k-vector indices in the x-, y- and z-directions of k_{max} = 7. The k-vector indices were truncated for $k^2 \le k_{max}^2 + 2$.[38]

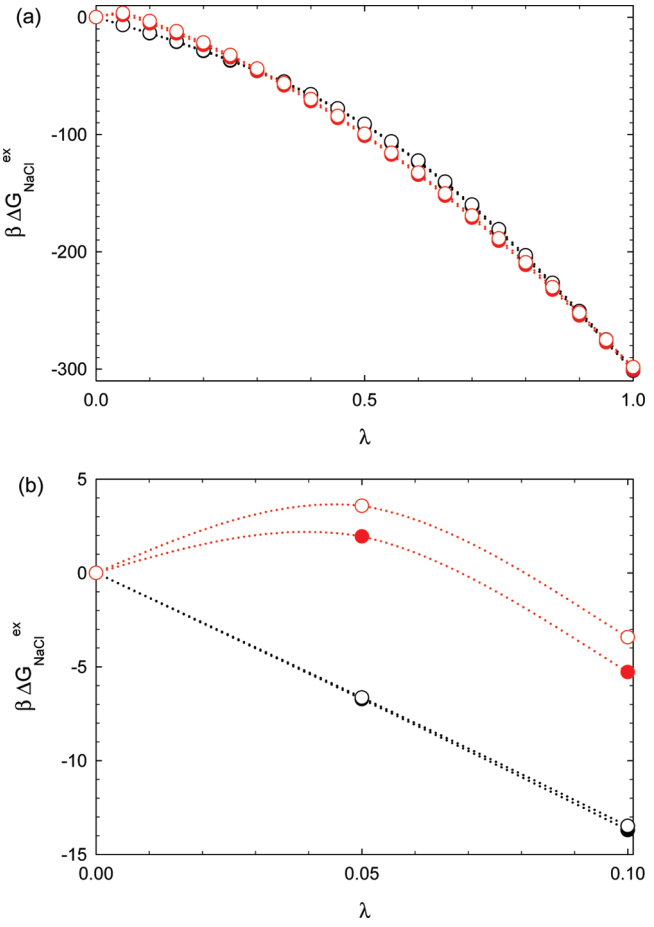

Figure 1. The dimensionless excess partial Gibbs free energy change, $\beta\Delta G^{ex}_{NaCl}$ in eq 28, associated with varying the coupling parameter λ from 0 to 1, for model 1 of aqueous NaCl at $T = 298.15$ K, $P = 1$ bar at a low and a high concentration. $\beta = 1/k_BT$, where k_B is Boltzmann's constant. Symbols represent the simulation results and the curves are rough guides to the eye. Black symbols and curves correspond to the scaling procedure of this work (eqs 20 and 21), while red symbols and curves represent linear scaling. The filled and open symbols correspond to molalities of $m = 0.2055$ and 4.7283 mol kg^{-1}, respectively. The concentration dependence is virtually indistinguishible for both scalings on the scale of the graph in part a and for the scaling of this work in part b.

To verify the accuracy of our OEMC simulations, we also directly calculated chemical potentials at selected concentrations using a multistage free energy perturbation (MFEP) method[6,39,40] in the *NPT* ensemble, described in the Appendix.

Equilibration for the OEMC simulations typically consisted of up to 2×10^8 MC trial moves, while production runs took about 2×10^9 MC trial moves. In the case of the MFEP calculations, $\exp(-\beta\Delta U)$ accumulators were zeroed after 5×10^7 and then again after 2×10^8 MC trial moves. This allowed us to verify that our results were not affected by the initial configuration.

5. RESULTS AND DISCUSSION

5.1. Scaling. It is important to examine the effects of the scaling procedure on the efficiency of the simulation. A complete examination of the efficiency of different scaling schemes requires careful statistical analysis and computations of uncertainties. Nevertheless, the dimensionless partial excess Gibbs free energy change, $\beta\Delta G^{ex}_{NaCl}(\lambda)$, which characterizes the coupling of fractional ions to the system, is a useful indicator of the performance of different scaling schemes. $\beta\Delta G^{ex}_{NaCl}(\lambda)$ is defined by

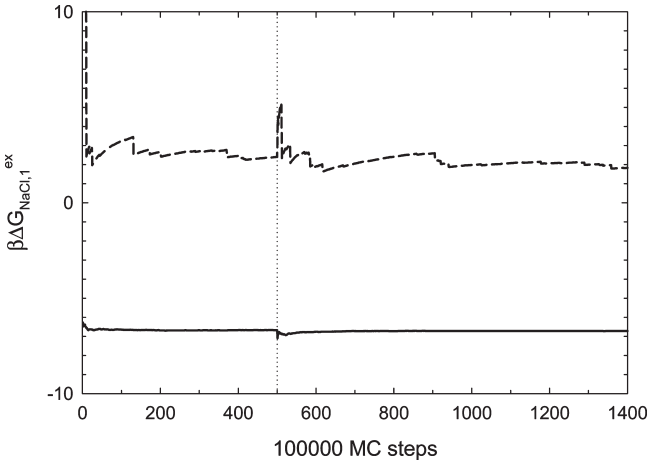

Figure 2. Convergence of the dimensionless excess Gibbs free energy difference between the neighboring λ-states 0 and 0.05, $\beta\Delta G^{ex}_{NaCl,1}$, calculated by our MFEP approach at $T = 298.15$ K, $P = 1$ bar, $m = 0.2055$ mol kg^{-1}, for the scaling of this work (solid curve) and for linear scaling (dashed curve), in the equilibration and production periods. The dotted vertical line indicates the boundary between the equilibration and production periods. At this boundary, the accumulators were zeroed to avoid contributions from nonequilibrium configurations to the final averages.

$$\beta\Delta G^{ex}_{NaCl}(\lambda_j) = \sum_{k=1}^{j} \beta\Delta G^{ex}_{NaCl,k} \qquad (28)$$

where $\Delta G^{ex}_{NaCl,k}$ is the excess Gibbs free energy difference between neighboring λ-states k and $k-1$. The variation with λ may indicate potential problems over particular regions of λ. Analysis of the behavior of $\beta\Delta G^{ex}_{NaCl}(\lambda)$ can be accompanied by analysis of the behavior of other quantities, e.g., radial distribution functions, to reveal any artifacts introduced by the scaling, such as "sticking" of fractional ions to water atoms at small values of λ. Examination of $\beta\Delta G^{ex}_{NaCl}(\lambda)$ can also help to choose a better λ-staging procedure for a given scaling procedure, since changes of $\beta\Delta G^{ex}_{NaCl}(\lambda)$ between neighboring λ-states should be roughly comparable, and a denser λ-staging can be indicated when $\beta\Delta G^{ex}_{NaCl}(\lambda)$ exhibits rapid changes.

Figure 1 compares $\beta\Delta G^{ex}_{NaCl}(\lambda)$ for our scaling procedure (eqs 20 and 21) with a commonly used linear scaling (used, for example, by Paluch et al.[16]), at a typical low and a typical high NaCl concentration for model 1. We calculated the values of $\beta\Delta G^{ex}_{NaCl,k}$ using a MFEP method[6,39,40] described in the Appendix.

Figure 1a also gives the total excess NaCl chemical potential, $\beta\mu^{ex}_{NaCl} = \beta\Delta G^{ex}_{NaCl}(1) - \beta\Delta G^{ex}_{NaCl}(0)$, as calculated by MFEP at the low and high concentrations. It exhibits a fairly small dependence on concentration, both for the scaling of this work and for linear scaling. Although indiscernible on the scale of the graph, the values are $\beta\mu^{ex}_{NaCl} = -301.35(2)$ at the low concentration ($m = 0.2055$ mol kg^{-1}) and $\beta\mu^{ex}_{NaCl} = -299.14(2)$ at the high concentration ($m = 4.7283$ mol kg^{-1}).

Figure 1a appears to indicate that $\beta\Delta G^{ex}_{NaCl}(\lambda)$ is relatively insensitive to the different scalings and that both scaling choices

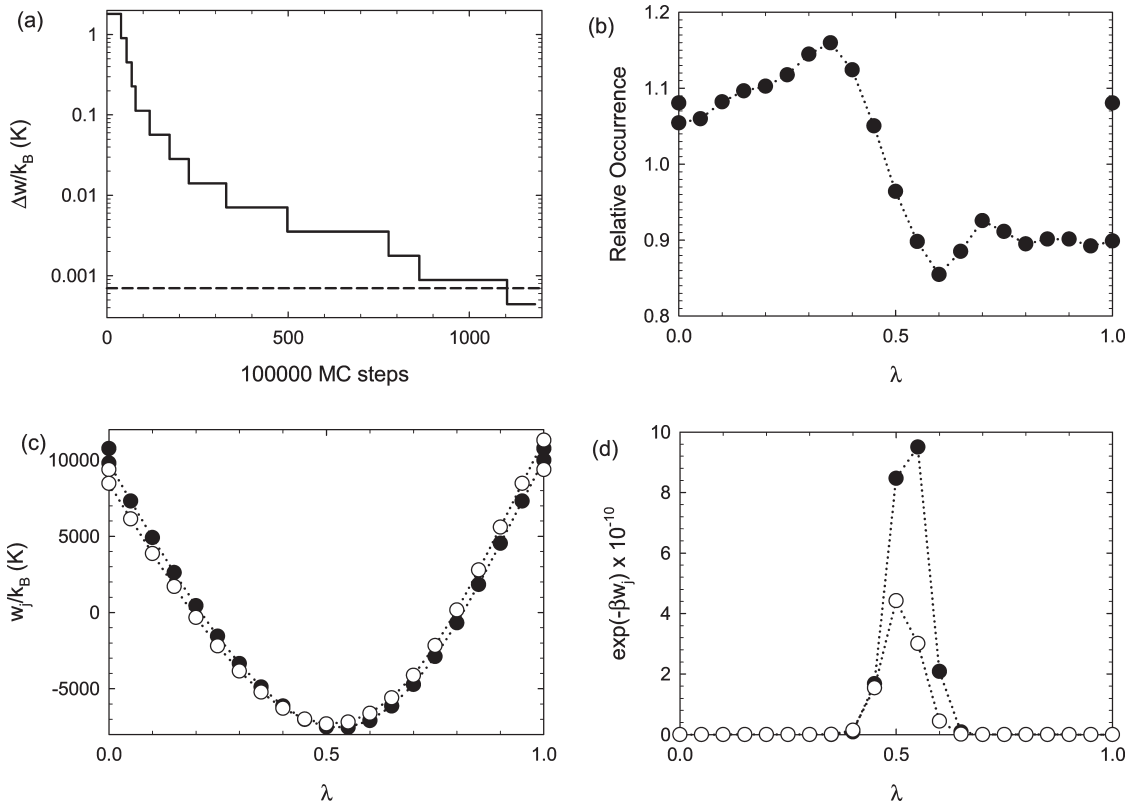

Figure 3. (a) The Wang−Landau parameter, Δw, as a function of the number of MC steps, and (b) the relative occurrence of the λ-states, both at $T = 298.15$ K, $P = 1$ bar, for $\tilde{\mu}_{NaCl} = -384.024$ kJ mol^{-1}. Panels c and d respectively show the weight functions, w_j, and the probability factors, $\exp(-\beta w_j)$, as a function of the coupling parameter λ for model 1 of aqueous NaCl at $T = 298.15$ K, $P = 1$ bar. Closed circles correspond to $\tilde{\mu}_{NaCl} = -414.024$ kJ mol^{-1} and open circles to $\tilde{\mu}_{NaCl} = -384.024$ kJ mol^{-1}, respectively corresponding to low and high concentrations of $m \simeq 0.1$ and 4.8 mol kg^{-1}. The dotted curves are guides to the eye only.

are similarly effective. However, Figure 1b reveals significant differences between them in the low λ range; whereas $\beta\Delta G^{ex}_{NaCl}(\lambda)$ for the scaling of this work is always negative and smoothly decreases with increasing λ, $\beta\Delta G^{ex}_{NaCl}(\lambda)$ for linear scaling is positive for $\lambda < 0.07$ and negative elsewhere. The positive region of $\beta\Delta G^{ex}_{NaCl}(\lambda)$, with a maximum value of about $4k_BT$ around $\lambda \simeq 0.05$, is associated with a fast coupling of the repulsive part of the ion short-range interactions and the necessity of creating a cavity in the solution.[41] This behavior can potentially indicate the inefficiency of the linear scaling scheme.

Differences between the scaling of this work and linear scaling within $\lambda \in (0, \sim 0.07)$ are further elaborated in Figure 2, which shows convergence profiles for $\beta\Delta G^{ex}_{NaCl,1}$ (between the neighboring λ-states at $\lambda = 0$ and $\lambda = 0.05$), during the equilibration and production periods of a typical simulation. Whereas $\beta\Delta G^{ex}_{NaCl,1}$ converges very quickly for the scaling of this work, convergence of $\beta\Delta G^{ex}_{NaCl,1}$ for the linear scaling is slow and not very smooth, resulting in a large statistical uncertainty and questionable accuracy of the ultimately calculated chemical potential. The poorer performance of linear scaling relative to that of nonlinear scaling in the region of $\lambda < 0.07$ is also evidenced by the relatively small values of acceptance ratios for λ-changes in Figure 4b over this region.

5.2. Biasing Weights. The determination of the biasing weights, w_j, and their effects on the simulations are shown in Figures 3 and 4 for model 1. Figure 3a shows a typical convergence behavior of the WL method for the parameter Δw used for the adjustment of w_j in eq 23, as a function of the number of MC steps. We see that the number of MC steps needed for properly collecting histograms of λ-states occurring at particular Δw-values increases with decreasing Δw, and a converged value of 7×10^{-4} K is reached after about 1×10^8 MC steps.

The resulting relative occurrences of the λ-states, the final values of w_j, and their corresponding probability factors $\exp(-\beta w_j)$ at two values of the overall NaCl chemical potential, μ_{NaCl}, corresponding to typical low and high concentrations, are displayed in parts b, c, and d of Figure 3, respectively.

The relative occurrence of each λ-state (Figure 3b) is not perfectly flat, but nevertheless, all the values lie within the interval (0.8, 1.2). The converged w_j-values (Figure 3c) span a rather wide range, with a minimum near $\lambda \simeq 0.5$. Similarly as for $\beta\Delta G^{ex}_{NaCl}(\lambda)$ in Figure 1, the w_j-values are not strongly dependent on concentration, and differences between both sets of w_j-values are just a few percent. These small differences, however, translate to very different values for the probability factors $\exp(-\beta w_j)$, as shown in Figure 3d, where we see enormous differences between the values of $\exp(-\beta w_j)$ at the two different concentrations for particular λ-states, with maximum values of about 9.6×10^{10} at the low concentration and about 4.5×10^{10} at the high concentration, both located near $\lambda = 0.5$. It is worthwhile noting that in an illustrative example of a LJ fluid considered in the CFC MC method,[23] a maximum value of $\exp(-\beta w_j)$ is 365.04, about 8 orders of magnitude smaller than for our aqueous NaCl system. This clearly demonstrates that it would be impossible to perform an efficient random walk in the λ-states without a proper choice of the biasing weights.

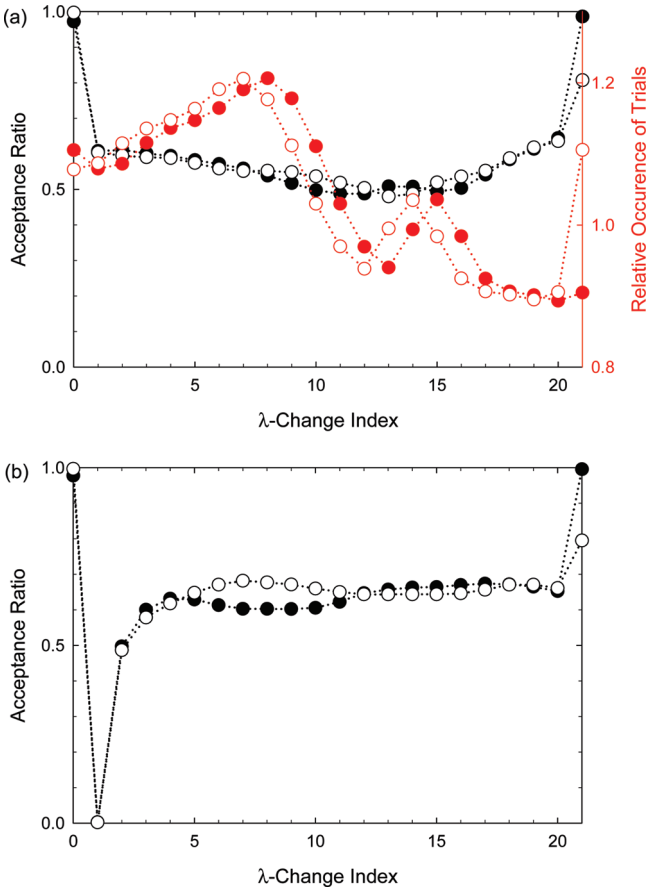

Figure 4. (a) Acceptance ratios for the λ-changes and the relative occurrence of λ-change trials in the forward (filled circles) and reverse (open circles) directions for the scaling of this work (eqs 20 and 21) and (b) acceptance ratios for λ-changes in the forward and reverse directions for linear scaling, in the case of model 1 for aqueous NaCl at $T = 298.15$ K, $P = 1$ bar, and $\mu_{NaCl} = -384.024$ kJ mol^{-1}, corresponding to a concentration of about 4.8 mol kg^{-1}. The horizontal axis refers to the change from λ_i to λ_{i+1} in the forward direction and from λ_{i+1} to λ_i in the reverse direction. See also eq 13. The dotted curves are guides to the eye only. In part a, black lines and symbols correspond to acceptance ratios for λ-changes, while red curves and symbols represent the relative occurrence of λ-change trials.

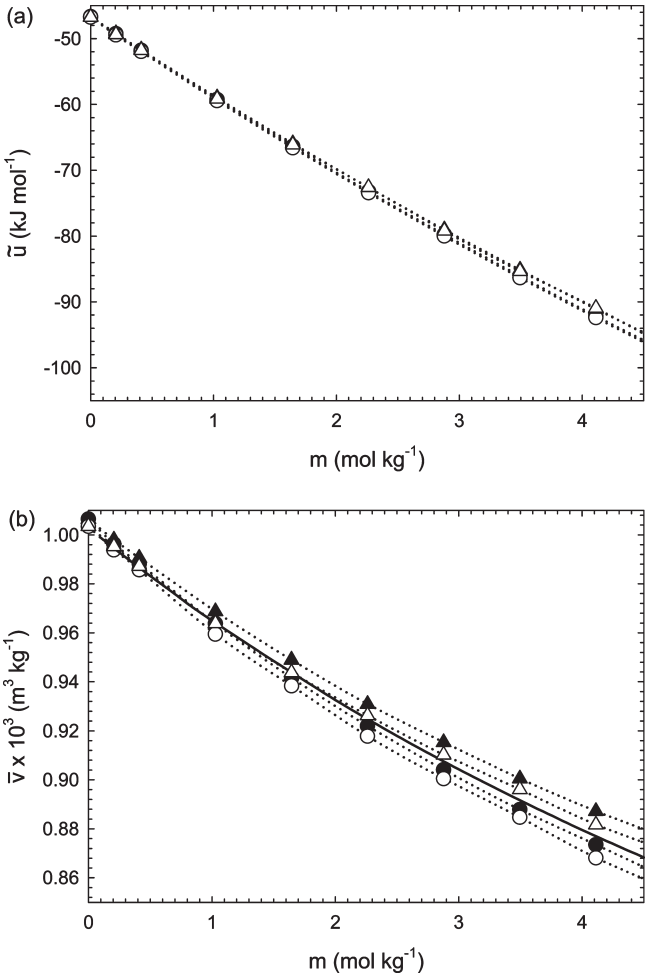

Figure 5. (a) The total molar configurational energy $\tilde{u}$ and (b) specific volume $\bar{v}$ as a function of molality m for an aqueous NaCl solution at $T = 298.15$ K and $P = 1$ bar. Circles and triangles denote models 1 and 2, respectively; filled symbols correspond to the GRF method and open symbols correspond to the ES technique. The solid curve represents the experimental values.[43] The dotted curves are guides to the eye only.

Figure 4 compares the acceptance ratios for λ-changes and the relative occurrence of λ-change trials in the forward and backward directions for our scaling and for linear scaling. For our scaling (Figure 4a), the acceptance ratios lie between 0.6 and 0.7 and the relative occurrences of the λ-change trials are relatively flat, corresponding to an acceptable choice of λ-scaling and λ-staging; for linear scaling (Figure 4b), the acceptance ratio is very small for λ-change 1 (about 0.002), which sharply contrasts with the change from $\lambda = 0$ to $\lambda = 0.05$, but otherwise the acceptance ratios are around 0.6. This small acceptance ratio for linear scaling around $\lambda = 0$ presents a bottleneck during the λ-walk in the simulation and is associated with the positive portion of $\beta\Delta G^{ex}_{NaCl}(\lambda)$ in Figure 1b. Removing the bottleneck while retaining linear scaling would require employing denser λ-staging around $\lambda = 0$, increasing the computational cost of the simulations.

5.3. GRF and ES Comparison. Although our implementation of the OEMC method uses the GRF approach for treatment of the long-ranged Coulombic interactions, we also compared our results with those obtained using the ES technique. We implemented the ES employing our scaling procedure only for the real part of the configurational energy. For the Fourier part, we only scaled the charges, since our expression of this part is not a function of intermolecular distance r. It may thus be possible to improve the efficiency of our ES implementation.

Since implementation of the ES technique within MC methods is not straightforward, we first developed our ES MC code from appropriate modifications to our OEMC code and validated it against two independently developed computer codes. We first compared values of the configurational energy and density at various NaCl concentrations from our ES code with *NPT* MD simulation results obtained using the freely available DL_POLY code.[42] We obtained agreement within statistical uncertainties for these quantities. Second, we compared our $\beta\mu_{NaCl}$ results using ES with those obtained from the independently developed computer code used for the EEOMD method [see Table 3 in ref 18 (not shown here)] and again obtained agreement within statistical uncertainties.

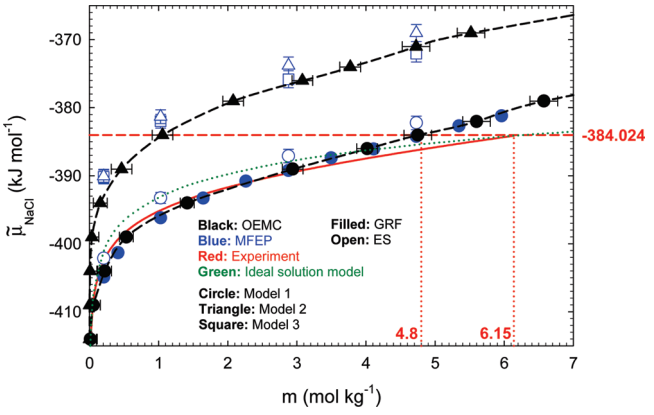

Figure 6. The molar electrolyte chemical potential $\tilde{\mu}_{NaCl}$ as a function of molality m, for aqueous NaCl at T = 298.15 K and P = 1 bar. Circles, triangles, and squares represent models 1, 2, and 3, respectively; filled symbols correspond to the GRF method and open symbols correspond to the ES technique. The black, blue, red, and green colors represent values obtained from OEMC, MFEP, experiment,[45] and Henry convention ideal solution model (eq 30), respectively. The red dashed horizontal line denotes the chemical potential of NaCl(s).[30] The black dashed curves are guides to the eye only. The computed precisions of the simulation results are within the symbols unless otherwise indicated on the graph.

Figure 5 compares the GRF and ES results for the molar configurational energy, $\tilde{u}$, and the specific volume, $\overline{v}$, for models 1 and 2, as a function of the NaCl solution concentration. Figure 5a shows that the differences between $\tilde{u}$ calculated by ES and by GRF are negligible and that the differences between the model results are quite small. In contrast, Figure 5b shows that the GRF and ES methods for a given model give somewhat different results for $\overline{v}$ and that the model differences are slightly larger. The differences between the ES and the GRF methods are relatively independent of the NaCl concentration, with the GRF method giving higher values of $\overline{v}$ (and hence lower values of density) than the ES method. (The experimental values of $\overline{v}$[43] are close to the ES results at m < 0.5 mol kg^{-1}; they are located between the results of the two molecular models at m > 2 mol kg^{-1} and they are the closest to the results of model 1 and GRF at m > 3 mol kg^{-1}.)

5.4. $\mu-m$ Curves and Solubility of NaCl. Figure 6 displays $\mu-m$ curves for an aqueous NaCl solution at T = 298.15 K and P = 1 bar as a function of concentration, for several model potentials and for GRF and ES treatments of the long-ranged Coulombic forces; also shown for comparison are experimental data[45] and values obtained by the Henry convention ideal solution model (ref 10, pp 52−55).

The total ionic molar chemical potential $\tilde{\mu}_{NaCl}$ was evaluated as (see also Appendix, eq A-7)

$$\tilde{\mu}_{NaCl} = \tilde{\mu}^0_{Na^+} + \tilde{\mu}^0_{Cl^-} + \frac{2N_A}{\beta} \ln\left(\frac{x_{NaCl}}{\beta P^0 v}\right) + \tilde{\mu}^{ex}_{NaCl} \qquad (29)$$

where $\tilde{\mu}^{ex}_{NaCl} = N_A \Sigma_{k=1}^{M} \Delta G^{ex}_{NaCl,k}$, and $\tilde{\mu}^0_{Na^+}$ and $\tilde{\mu}^0_{Cl^-}$ are the molar standard chemical potentials of the Na^+ and Cl^- ions, respectively. The standard chemical potential values are taken from the NIST-JANAF tables[30] as free energy of formation values: $\tilde{\mu}_{Na^+}{}^0$ = 574.317 kJ mol^{-1} and $\tilde{\mu}_{Cl^-}{}^0$ = −240.167 kJ mol^{-1}. The value of $\tilde{\mu}_{NaCl}$ for NaCl(s) as given by the NIST-JANAF tables, $\tilde{\mu}^{JANAF}_{NaCl(s)}$ = −384.024 kJ mol^{-1}, is also indicated in the figure. [In our previous paper on the aqueous NaCl system,[18] numerical values of $\tilde{\mu}^0_i$ using the enthalpy of formation at the reference temperature T_r = 298.15 K, $\tilde{h}_i = \Delta H_{fi}(T_r)$; the absolute entropy at T_r, $\tilde{s}^0_i(T_r)$; and the ideal-gas heat capacity, $\tilde{c}^0_{Pi}(T)$, using

$$\tilde{\mu}^0_i(T) = \tilde{h}^0_i(T) - T\tilde{s}^0_i(T)$$

where

$$\tilde{h}^0_i(T) = \Delta H_{fi}(T_r) + \int_{T_r}^{T} \tilde{c}^0_{Pi}(T)\, dT$$

$$\tilde{s}^0_i(T) = \tilde{s}^0_i(T_r) + \int_{T_r}^{T} \frac{\tilde{c}^0_{Pi}(T)}{T}\, dT$$

were evaluated.] The value of v was obtained from an *NPT* simulation with no fractional ions. For our OEMC method, μ_{NaCl} is an input parameter, and the concentration of the ions is determined by the simulation. We also show *NPT* MC simulation results utilizing both the GRF and ES methods; we also separately determined μ_{NaCl} in the former case by the MFEP method, providing a check for the consistency of the OEMC results.

We first note that Figure 6 shows excellent agreement between the OEMC and MFEP results obtained using the GRF method (black and blue filled circles), giving confidence in the accuracy of our results and the correctness of our computer algorithms. The most important aspect of the figure is that our results for model 1 reproduce reasonably well the experimental $\mu_{NaCl}-m$ curve over the entire concentration range (particularly for the GRF results up to $m \approx 3$). The experimental $\mu_{NaCl}-m$ curve is seen to be significantly overpredicted by both model 2 and model 3. The MFEP with the ES method gives only slightly higher values of $\tilde{\mu}_{NaCl}$ in comparison with the GRF method (open and filled circles for model 1 and open and filled triangles for model 2). Such relatively small differences between the results of the GRF and ES methods seem to play a much less important role than differences between the force field models. For example, differences in the $\tilde{\mu}_{NaCl}-m$ curves for model 1 and model 2 are typically about 14 kJ mol^{-1}, whereas corresponding differences between the GRF and ES methods are less than 2 kJ mol^{-1}.

We note that Figure 6 displays a fairly small chemical potential range (≈40 kJ mol^{-1}) in comparison with the numerical values. This results in a considerable sensitivity of the computed value of the solubility to the details of the models. Nevertheless, the solubility predicted by model 1 is m = 4.8(3) mol kg^{-1}, which compares reasonably well with the experimental value of m = 6.1 mol kg^{-1}.[45] Note that the solubility is determined via a single simulation at the specified solid chemical potential. We also note that the OEMC GRF results are shown down to very low concentrations, which would not be feasible to determine using the closed system MFEP method.

Model 3 predicts a concentration dependence of $\tilde{\mu}_{NaCl}$ that agrees within statistical uncertainties with that of our model 2 results in the low concentration region; at higher concentrations, the results differ, likely due to differences between the ion−ion interaction portions of these models.

The electrolyte chemical potential may be expressed according to the Henry convention as

$$\tilde{\mu}_{NaCl} = \tilde{\mu}^{Ideal,H}_{NaCl} + 2RT \ln \gamma^{H}_{NaCl}$$

where R is the universal gas constant, γ^{H}_{NaCl} is the Henry convention mean ion activity coefficient of Na^+ and Cl^- in

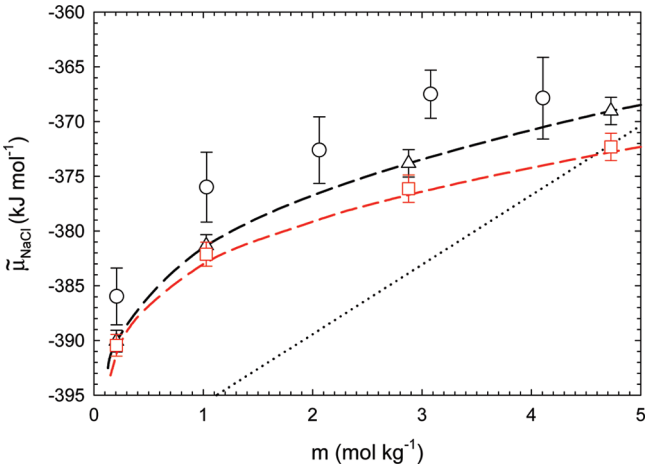

Figure 7. Comparison of the molar chemical potential vs concentration ($\tilde{\mu}_{NaCl}$−m) curves for P = 1 bar from this work using the MFEP and ES techniques for model 2 at T = 298.15 K (triangles) and for model 3 at T = 300 K (squares), with the results of previous authors: Paluch et al.[16] (circles) and Sanz and Vega[13] (dotted line), both for T = 298 K, and Lisal et al.[18] for T = 300 K (red dashed curve). The black dashed curve is a guide to the eye only.

the solution, and $\tilde{\mu}_{NaCl}^{Ideal,H}$ is the Henry convention ideal solution chemical potential:

$$\tilde{\mu}_{NaCl}^{Ideal,H} = \tilde{\mu}_{Na^+}^{\dagger} + \tilde{\mu}_{Cl^-}^{\dagger} + 2RT\ln m_{NaCl} \qquad (30)$$

where $\tilde{\mu}_{Na^+}^{\dagger}$ and $\tilde{\mu}_{Cl^+}^{\dagger}$ are experimentally determined values, given in the NBS tables.[46] $\tilde{\mu}_{NaCl}^{Ideal,H}$ agrees well with the experimental curve at m < 0.1 mol kg^{-1}; it is about 3 kJ mol^{-1} higher at $m \approx 2$ mol kg^{-1}, and it crosses the experimental curve at $m \approx 6$ mol kg^{-1}. The ideal solution model thus predicts the solubility of NaCl well; however, this is a coincidence in the case of NaCl, since γ_{NaCl}^{H} is close to unity at the solubility limit $m \approx 6.15$.[45] The activity coefficients of other salts exhibit quite different behaviors; e.g., the activity coefficients of the ions in saturated aqueous solutions are 0.589 for KCl and 3.8 for KF.[45] It should also be noted that the values of $\tilde{\mu}^{\dagger}$ for the ions are directly related to the hydration free energies, which may be determined by computer simulation if the experimental values are not known.

Finally, in Figure 7, we compare our μ_{NaCl} calculations for model 3 with our previously obtained results[18] and with the results of Sanz and Vega[13] and of Paluch et al.[16] Our results agree with those of our previous calculations, obtained using independently developed computer codes. The results of Paluch et al. and Sanz and Vega were obtained at a slightly different temperature. However, it can be seen that our results are generally consistent with those of Paluch et al.[16] and at variance with those of Sanz and Vega.[13]

6. CONCLUSIONS

We have presented a novel molecular simulation tool, the osmotic ensemble Monte Carlo (OEMC) method, for the computationally efficient calculation of the properties of aqueous electrolyte solutions, particularly those involving free energy.

In comparison with previous methods, our OEMC approach has several advantages:

(1) The method greatly facilitates the calculation of solubility, which is obtained directly as the output equilibrium concentration from a single molecular simulation; the solubility is calculated as the concentration resulting from setting the overall solute chemical potential to that of the corresponding crystalline solid.
(2) The method allows calculation of the free energy−concentration curve over a continuous range that includes the low concentration region, which is inaccessible using simulations in closed ensembles.
(3) The method avoids simulations of the solid phase, incorporating readily available data from thermochemical tables that are based on well-defined reference states.
(4) The method can be easily extended to the case of multiple electrolytes and other solutes present simultaneously in the solution and to cases when complexation reactions must also be considered.

We tested the method using three representative molecular models for NaCl dissolved in water at ambient conditions. Standard chemical potentials from thermochemical tables were employed, which use clearly defined reference states. This obviates the need for simulations of the solid phase and readily allowed direct comparison of the results with experimental data. Our OEMC simulations showed excellent agreement with our independent calculations of NaCl chemical potentials in water performed by the MFEP method, verifying the accuracy of our approach. Our calculations using the SPC/E water model in conjunction with the ionic force field model of Joung and Cheatham[17] achieved good agreement with experimental results for the chemical potential−concentration curve and reasonable agreement for the solubility. To our knowledge, the chemical potential−concentration curve obtained using model 1 in Figure 6 is the most accurate molecular-level-based prediction of this property published to date.

Finally, our results indicate that the primary source of improved predictions from our calculations will arise from improvements to the molecular models employed. In future work, we will explore such improvements and extend our methodology to calculate the solubilities and free energy−concentration curves of other electrolytes.

APPENDIX

This appendix describes a MFEP method[6,39] used for the calculation of the overall electrolyte chemical potential for aqueous 1:1 electrolyte solutions, μ_{AB}, in NPT simulations at a specified electrolyte concentration. In the NPT ensemble, the dimensionless Gibbs free energy change, $\beta\Delta G$, of a process changing the number of particles of type i, N_i, by ΔN_i (resulting in a change in the dimensionless system configurational energy βU by $\beta\Delta U$) is given by

$$\beta\Delta G = -\ln\frac{\overline{Q}_{NPT}}{Q_{NPT}}$$

$$= -\ln\frac{\prod_{i=1}^{s}\frac{q_i^{N_i+\Delta N_i}}{(N_i+\Delta N_i)!\Lambda_i^{3(N_i+\Delta N_i)}}}{\prod_{i=1}^{s}\frac{q_i^{N_i}}{N_i!\Lambda_i^{3N_i}}}$$

dx.doi.org/10.1021/jp202054d |J. Phys. Chem. B 2011, 115, 7849–7861

$$-\ln\frac{\int dV\, V^{N+\Delta N}\exp(-\beta PV)\int d\{\xi,\omega\}^{N+\Delta N}\exp[-\beta(U+\Delta U)]}{\int dV\, V^{N}\exp(-\beta PV)\int d\{\xi,\omega\}^{N}\exp(-\beta U)}$$

$$= -\ln\prod_{i=1}^{s}\frac{N_i!q_i^{\Delta N_i}}{(N_i+\Delta N_i)!\Lambda_i^{3\Delta N_i}} - \ln\left\langle V^{\Delta N}\int d\{\xi,\omega\}^{\Delta N}\exp(-\beta\Delta U)\right\rangle_{NPT}$$

$$= -\ln\prod_{i=1}^{s}\frac{N_i!q_i^{\Delta N_i}}{(N_i+\Delta N_i)!\Lambda_i^{3\Delta N_i}} - \ln\left\langle V^{\Delta N}\langle\exp(-\beta\Delta U)\rangle_{\{\xi,\omega\}^{\Delta N}}\right\rangle_{NPT} \quad \text{(A-1)}$$

where s is the number of species, Q_{NPT} and $\overline{Q}_{NPT}$ respectively are the partition function before and after the ΔN_i change, $\langle\ \rangle$ is an ensemble average corresponding to Q_{NPT}, V is the volume, P is the pressure, $\beta = 1/k_BT$, k_B is Boltzmann's constant, T is the temperature, q_i and Λ_i respectively are the internal partition function and thermal de Broglie wavelength of species i, N is the total number of particles, $\Delta N = \Sigma\Delta N_i$, and ξ and ω are the reduced particle positions and molecule rotations, respectively. Using

$$\frac{q_i}{\Lambda_i^3} = \beta P^0\exp(-\beta\mu_i^0) \quad \text{(A-2)}$$

where μ_i^0 is the standard chemical potential per particle of species i and P^0 is the standard-state pressure. We obtain for ΔG:

$$\beta\Delta G = \beta\sum_{i=1}^{s}\mu_i^0\Delta N_i - \sum_{i=1}^{s}\ln\left[\frac{N_i!}{(N_i+\Delta N_i)!}(\beta P^0)^{\Delta N_i}\right] - \ln\left\langle V^{\Delta N}\langle\exp(-\beta\Delta U)\rangle_{\{\xi,\omega\}^{\Delta N}}\right\rangle_{NPT} \quad \text{(A-3)}$$

For the insertion of an ion pair A^+ and B^- to the aqueous solution of N_w water molecules and N_{AB} ion pairs, we have

$$\beta\Delta G_{AB} \equiv \beta\mu_{AB} = \beta(\mu_{A^+}^0+\mu_{B^-}^0) - 2\ln\frac{\beta P^0}{N_{AB}+1} - \ln\left\langle V^2\langle\exp(-\beta\Delta U)\rangle_{\{\xi,\omega\}^2}\right\rangle_{NPT} \quad \text{(A-4)}$$

where $N_{AB} = N_{A+} = N_{B-}$. $\beta\mu_{AB}$ can be expressed as a sum of ideal and excess contributions, $\beta\mu_{AB}^{IG}$ and $\beta\mu_{AB}^{ex}$, respectively, as

$$\beta\mu_{AB}^{IG} = \beta\mu_{A^+}^0+\beta\mu_{B^-}^0 - 2\ln\left(\frac{\beta P^0}{N_{AB}+1}\right) - \ln\langle V^2\rangle_{NPT} \quad \text{(A-5)}$$

$$\beta\mu_{AB}^{ex} = -\ln\left(\frac{\left\langle V^2\langle\exp(-\beta\Delta U)\rangle_{\{\xi,\omega\}^2}\right\rangle_{NPT}}{\langle V^2\rangle_{NPT}}\right) \quad \text{(A-6)}$$

(This definition of $\beta\mu^{ex}$ corresponds to $\beta\mu^{ex}(T,V)$; see eq 8 of ref 41). In the thermodynamic limit, where the number of particles in the system approaches infinity, $N_{AB}+1 \rightarrow N_{AB}$, $(\langle V^2\rangle_{NPT} - \langle V\rangle_{NPT}{}^2)/\langle V\rangle_{NPT}{}^2 \rightarrow 0$ (see pp 37−38 of ref 47), and it is straightforward to show that the ideal contribution to $\beta\mu_{AB}$ becomes

$$\beta\mu_{AB}^{IG} = \beta\mu_{A^+}^0+\beta\mu_{B^-}^0 + 2\ln\frac{N_{AB}}{\beta P^0\langle V\rangle_{NPT}} = \beta\mu_{A^+}^0+\beta\mu_{B^-}^0 + 2\ln\frac{x_{AB}}{\beta P^0 v} \quad \text{(A-7)}$$

where $x_{AB} = N_{AB}/N$ and $v = \langle V\rangle_{NPT}/N$.

Due to the essentially zero probability of insertion/deletion of an ion pair to/from the system, use of eq A-6 is impractical. Instead, we choose a λ-scaling and λ-staging procedure and calculate the contributions from each λ-state utilizing eq A-3 and extract the excess term:

$$\beta\Delta G_{AB,k}^{ex} = -\ln\frac{\left\langle V^{\Delta N}\langle\exp(-\beta\Delta U)\rangle_{\{\xi,\omega\}^{\Delta N}}\right\rangle_{NPT}}{\langle V^{\Delta N}\rangle_{NPT}} \quad \text{(A-8)}$$

$\beta\mu_{AB}^{ex}$ is then given by

$$\beta\mu_{AB}^{ex} = \sum_{j=1}^{M}\beta\Delta G_{AB,j}^{ex} \quad \text{(A-9)}$$

where M is the total number of λ-states. We calculated the terms in the summation of eq A-9 by means of a parallel computation using $M = 20$.

AUTHOR INFORMATION

Corresponding Author
*E-mail: william.smith@uoit.ca.

ACKNOWLEDGMENT

Support for this work was provided by the Natural Sciences and Engineering Research Council of Canada (Grant No. OGP1041), the Ontario Research Fund, the SHARCNET grid computing facility (http://www.SHARCNET.ca), the Grant Agency of the Czech Republic (Grant No. 203/08/0094), the Grant Programme of the Academy of Sciences of the Czech Republic "Nanotechnology for Society" (Project No. KAN400720701), and the European Community under the seventh Framework Programme (Project COST TD0802).

REFERENCES

(1) Palmer, D. A.; Fernández-Prini, R.; Harvey, A. H. *Aqueous Systems at Elevated Temperatures and Pressures*; Elsevier: Amsterdam, 2004.
(2) Chialvo, A. A.; Gruszkiewicz, M. S.; Cole, D. R. *J. Chem. Eng. Data* **2010**, *55*, 1828–1836.
(3) Laudernet, Y.; Cartailler, T.; Turq, P.; Ferrario, M. *J. Phys. Chem. B* **2003**, *107*, 2354–2361.
(4) Uchida, H.; Matsuoka, M. *Fluid Phase Equilib.* **2004**, *219*, 49–54.
(5) Brodholt, J. P. *Chem. Geol.* **1998**, *151*, 11–19.
(6) Radmer, R. J.; Kollman, P. A. *J. Comput. Chem.* **1997**, *18*, 902–919.
(7) Lyubartsev, A. P.; Martsinovski, S. V.; Shevkunov, S. V.; Vorontsov-Velyaminov, P. N. *J. Chem. Phys.* **1992**, *96*, 1776–1783.
(8) Lyubartsev, A. P.; Førrisdahl, O. K.; Laaksonen, A. *J. Chem. Phys.* **1998**, *108*, 227–233.
(9) Westergren, J.; Lindfors, L.; Höglund, T.; Lüder, K.; Nordholm, S.; Kjellander, R. *J. Phys. Chem. B* **2007**, *111*, 1872–1882. Lüder, K.; Lindfors, L.; Westergren, J.; Nordholm, S.; Kjellander, R. *J. Phys. Chem. B* **2007**, *111*, 1883–1892. Lüder, K.; Lindfors, L.; Westergren, J.; Nordholm, S.; Kjellander, R. *J. Phys. Chem. B* **2007**, *111*, 7303–7311. Lüder, K.; Lindfors, L.; Westergren, J.; Nordholm, S.; Persson, R.; Pedersen, M. *J. Comput. Chem.* **2009**, *30*, 1859–1871.

(10) For example: Smith, W. R.; Missen, R. W. *Chemical Reaction Equilibrium Analysis: Theory and Algorithms*; Wiley-Intersicence: New York, 1982; reprinted with corrections, Krieger Publishing: Malabar, FL, 1991.
(11) Cui, S. T.; Harris, J. G. *J. Phys. Chem.* **1995**, *99*, 2900–2906.
(12) Ferrario, M.; Ciccotti, G.; Cartailler, T.; Spohr, E.; Turq, P. *J. Chem. Phys.* **2002**, *117*, 4947–4953.
(13) Sanz, E.; Vega, C. *J. Chem. Phys.* **2007**, *126*, 014507.
(14) Meijer, E. J.; Frenkel, D. *J. Chem. Phys.* **1990**, *92*, 7570–7575.
(15) Frenkel, D.; Smit, B. *Understanding Molecular Simulation: From Algorithms to Applications*; Academic Press: San Diego, CA, 2002.
(16) Paluch, A. S.; Jayaraman, S.; Shah, J. K.; Maginn, E. J. *J. Chem. Phys.* **2010**, *133*, 124504.
(17) Joung, I. S.; Cheatham, T. E., III *J. Phys. Chem. B* **2009**, *113*, 13279–13290.
(18) Lísal, M.; Smith, W. R.; Kolafa, J. *J. Phys. Chem. B* **2005**, *109*, 12956–12965.
(19) Joback, K. G.; Reid, R. C. *Chem. Eng. Commun.* **1987**, *57*, 233–243.
(20) Escobedo, F. A.; de Pablo, J. J. *J. Chem. Phys.* **1996**, *105*, 4391–4394.
(21) Çagin, T.; Pettitt, B. M. *Mol. Simul.* **1991**, *6*, 5–26. Çagin, T.; Pettitt, B. M. *Mol. Phys.* **1991**, *72*, 169–175. Ji, J.; Çagin, T.; Pettitt, B. M. *J. Chem. Phys.* **1992**, *96*, 1333–1342. Weerasinghe, S.; Pettitt, B. M. *Mol. Phys.* **1994**, *82*, 897–912. Lynch, G. C.; Pettitt, B. M. *J. Chem. Phys.* **1997**, *107*, 8594–8610. Lo, C.; Palmer, B. *J. Chem. Phys.* **1995**, *102*, 925–931. Shroll, R. M.; Smith, D. E. *J. Chem. Phys.* **1999**, *110*, 8295–8302. Shroll, R. M.; Smith, D. E. *J. Chem. Phys.* **1999**, *111*, 9025–9033. Morrow, T. I.; Maginn, E. J. *J. Chem. Phys.* **2005**, *122*, 054504. Morrow, T. I.; Maginn, E. J. *J. Chem. Phys.* **2006**, *125*, 204712. Boinepalli, S.; Attard, P. *J. Chem. Phys.* **2004**, *119*, 12769–12775.
(22) Lísal, M.; Brennan, J. K.; Smith, W. R. *J. Chem. Phys.* **2006**, *125*, 16490. Lísal, M.; Brennan, J. K.; Smith, W. R. *J. Chem. Phys.* **2009**, *130*, 104902.
(23) Shi, W.; Maginn, E. J. *J. Chem. Theory Comput.* **2007**, *3*, 1451–1463.
(24) Trebst, S.; Huse, D. A.; Troyer, M. *Phys. Rev. E* **2004**, *70*, 046701.
(25) Escobedo, F. A.; Martnez-Veracoechea, F. J. *J. Chem. Phys.* **2007**, *127*, 174103. Escobedo, F. A. *J. Chem. Phys.* **2007**, *127*, 174104.
(26) Escobedo, F. A.; Martnez-Veracoechea, F. J. *J. Chem. Phys.* **2008**, *129*, 154107.
(27) Wilding, N. B.; Müller, M. *J. Chem. Phys.* **1994**, *101*, 4324–4330.
(28) Wang, F.; Landau, D. P. *Phys. Rev. Lett.* **2001**, *86*, 2050–2053.
(29) Smith, W. R.; Tříska, B. *J. Chem. Phys.* **1994**, *100*, 3019–3027. Lísal, M.; Nezbeda, I.; Smith, W. R. *J. Chem. Phys.* **1999**, *110*, 8597–8604. Turner, C. H.; Brennan, J. K.; Lísal, M.; Smith, W. R.; Johnson, J. K.; Gubbins, K. E. *Mol. Simul.* **2008**, *34*, 119–146.
(30) Chase Jr., M. *NIST-JANAF Thermochemical Tables*; Journal of Physical and Chemical Reference Data Monograph No. 9; American Chemical Society and American Institute of Physics: Woodbury, NY, 1998.
(31) Pedley, J. B. *Thermodynamical Data and Structures of Organic Compounds*; TRC Data Series; Thermodynamic Research Center: College Station, TX, 1994.
(32) Hummer, G.; Pratt, L. R.; Garca, A. E. *J. Phys. Chem.* **1996**, *100*, 1206–1215.
(33) Allen, M. P.; Tildesley, D. J. *Computer Simulation of Liquids*; Clarendon Press: Oxford, 1987.
(34) McQuarrie, D. A. *Statistical Mechanics*; University Science Books: New York, 2000.
(35) Rowlinson, J. S. The Prefect Gas. *International Encyclopedia of Physical Chemistry and Chemical Physics*; MacMillan: New York, 1963; Topic 10, Vol. 5,
(36) Beutler, T. C.; Mark, A. E.; van Schaik, R. C.; Gerber, P. R.; van Gunsteren, W. F. *Chem. Phys. Lett.* **1994**, *222*, 529–539.
(37) Berendsen, H. J. C.; Grigera, J. R.; Straatsma, T. P. *J. Phys. Chem.* **1987**, *91*, 6269–6271.
(38) Kolafa, J.; Perram, J. *Mol. Simul.* **1992**, *9*, 351–368.
(39) Lu, N.; Kofke, D. A. *J. Chem. Phys.* **1999**, *111*, 4414–4423.
(40) Lu, N.; Singh, J. K.; Kofke, D. A. *J. Chem. Phys.* **2003**, *118*, 2977–2984.
(41) Lísal, M.; Smith, W. R.; Aim, K. *Fluid Phase Equilib.* **2004**, *226*, 161–172.
(42) Todorov, I. T.; Smith, W. *Philos. Trans. R. Soc. London A* **2004**, *362*, 1835–1852.
(43) Rogers, P. S. Z.; Pitzer, K. S. *J. Phys. Chem. Ref. Data* **1982**, *11*, 15–81.
(44) Smith, D. E.; Dang, L. X. *J. Chem. Phys.* **1994**, *100*, 3757–3766.
(45) Hamer, W. J.; Wu, Y.-C. *J. Phys. Chem. Ref. Data* **1972**, *1*, 1047–1099.
(46) Wagman, D. D. *J. Phys. Chem. Ref. Data* **1982**, *11*, supp. 2.
(47) Hill, T. T. *Introduction to Statistical Thermodynamics*; Addison-Wesley: Reading, 1960.